JOURNAL OF MATERIALS SCIENCE 7 (1972) 404–412

Secondary Processes in the Evolution of Sputter-Topographies

A. R. BAYLY
University of Sussex, School of Mathematical and Physical Sciences, Brighton, UK

Topographies of silica glass surfaces developed by 20 keV Ar^+ irradiation contain features which are not adequately explained by considering only the variation of sputtering yield with the ion-incidence angle. These features are sharply defined and could lead to serious misinterpretation of specimen structures when sputter-erosion is used as a microscopic sectioning technique. Three mechanisms are discussed which together could account for the observed discrepancies, the first being ion-reflection at grazing incidence, the second the phenomenon of forward-peaked emission of high-energy secondary particles under irradiation at high angles of incidence and the third being re-deposition of sputtered material onto closely adjacent planes. A general expression is derived for this latter mechanism for a cosine spatial distribution of sputtered particles.

1. Introduction

Low-energy heavy-ion sputtering has been the subject of extensive studies in physics while recently the technique has been applied to the sectioning of specimens for electron-microscope studies in such diverse fields as glass and ceramics [1], and diseased blood cells [2]. In such application it is necessary to distinguish between topographical effects which may arise even in structureless materials owing to the complexity of the sputtering mechanisms, and those due to the exposure of the structure sought. Numerous observations of relief effects in metallic or ionic crystals, and glasses or ceramics already have been published and an extensive review of the whole subject of sputtering is given by Carter and Colligon [3] while a short review of modern work on glass is given by Wilson [4], but there is still some doubt as to the origin of some features. This paper discusses some secondary sputtering processes which can lead to significant deviations of the topography from that implied by recent theoretical predictions [5, 6].

The experimental results discussed here arose from a requirement for damage-free optical flats on pure vitreous silica samples, the problem being, more specifically, to remove the Griffith-flawed layer remaining on surfaces finished by conventional polishing techniques. The Griffith flaws, not normally visible in a scanning electron microscope, become visible after etching the glass in dilute hydrofluoric acid (1%) for a few tens of minutes (fig. 1a) as fine fissures typically 1 to 10 μm long, and develop into hemi-spheroidal pits (fig. 1b) after several hours of etching. Experiments were conducted (a) to assess the possibility of removing the damaged layer by ion-sputtering the polished (i.e. not etched) surface, and (b) to test theoretical predictions of sputter-topographies developing from non-planar-surfaces, by studying the behaviour of the two types of pitted surface, formed by acid-etching (figs. 1a and b), under subsequent sputtering.

The three types of surface used in experiments (a) and (b) above were formed on a single sample by masked etching of a polished surface, so that the surfaces could be irradiated simultaneously under identical conditions, to identical ion-doses.

Irradiations were performed under high vacuum conditions with liquid nitrogen trapping (10^{-6} torr) using an analysed beam of Ar^+ 20 keV ions, current density 30 $\mu A/cm^2$, incident at 0° (i.e. normal to) to the sample face. The insulating glass surface was maintained electrically neutral during irradiation by simultaneous low-energy (< 100 eV) electron-irradiation. Ion current was measured before and after irradiation on a Faraday cup, and beam stability was monitored during irradiation on the defining aperture.

The silica specimens were grade "A" spectrosil

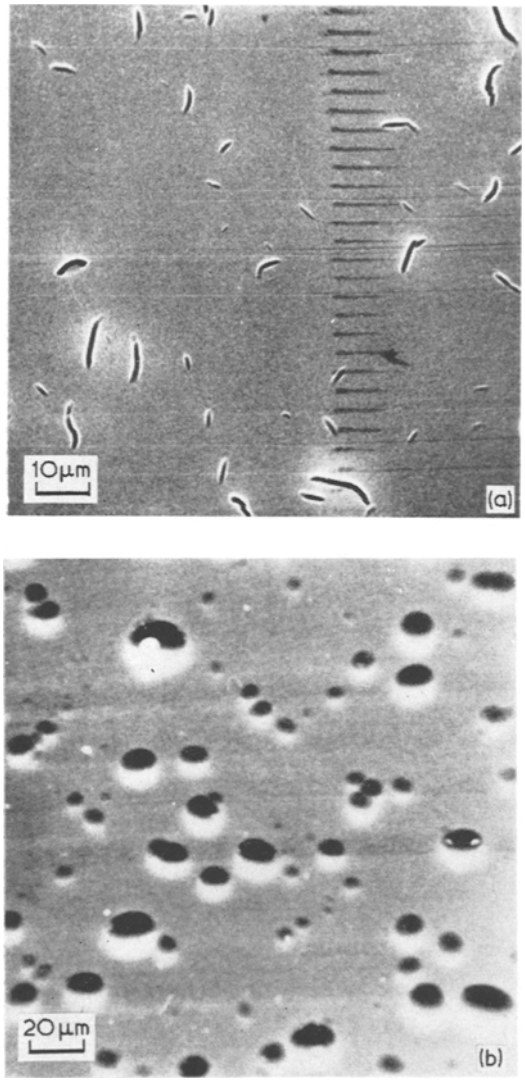

Figure 1 A polished silica glass surface after (a) 100 min and (b) 10 h etching, 2% HF. (N.B. The dark parallel lines seen in some photographs were markings on the stereoscan screen.)

fused synthetic silica supplied by Thermal Syndicate Ltd with quoted impurity levels of less than 0.2 ppm total content, the main species being Cr, P, Al, B, Fe, Zn.

2. The Nature of the Sputtered Surface

2.1. Polished Surfaces

The appearance of the polished surface after sputter-removal of about 0.7 μm (5×10^{18} ions/cm^2) was not noticeably altered except for a few ($\sim 10^2$/cm^2) small pits, usually "pill-box"-shaped with dimensions the order of a micron. Their shape (for reasons which appear later) and estimated combined volume suggest that they originate from bubbles, which are quoted as having a cross-section of $< 3 \times 10^{-6}$ cm^2/cm^3 by the manufacturers. However, by post-irradiation etching and counting flaw densities in irradiated and non-irradiated regions, the former were found to contain 30% fewer flaws than the latter (which contained $\sim 4 \times 10^5$/cm^2). It has previously been shown [7] on a larger scale, that an optically flat surface remains so after uniform sputtering.

2.2. Lightly Etched Surfaces

The narrow fissures produced by etching expanded out into steep-sided kidney-shaped troughs with widths typically about 4 μm and depths ranging from less than 1 μm up to several microns (see fig. 2). In the shallower troughs a smooth depression appeared in the central region of the otherwise flat base, while in the deep formations the steep sides were cut up into a regular staircase of terraces with steps about 1 μm in height (see fig. 3).

2.3. Heavily Etched Surfaces

The majority of pits, being fairly shallow, underwent no obvious changes in general appearance (fig. 4a). However, in the deeper pits, having steeper sides, sharply defined isolated steps appeared on the sides, with faces approximately parallel and normal to the incident beam (figs. 4a and b). The number density of such individual formations increased with increasing slope of the pit side and on the steepest-sided pits a continuous right-angled step was cut into the entire, or a major part of the circumference of the crater rim (fig. 4c).

3. Discussion

3.1. Theoretical Predictions

The recent interpretations [5, 6] of sputtered topographies stress the importance of the variation of sputtering coefficient with angle of incidence, a typical example for an "amorphous" material being that for silica under 5-6 keV Ar^+ bombardment [1] (fig. 5). Mathematical formalisms for the case of movements of intersections of planes [5] and for the more general case of the evolution of topographies from initially smoothly curved surfaces [6] predict the likely equilibrium surfaces evolving under monoenergetic, unidirectional ion fluxes. In general it is necessary to

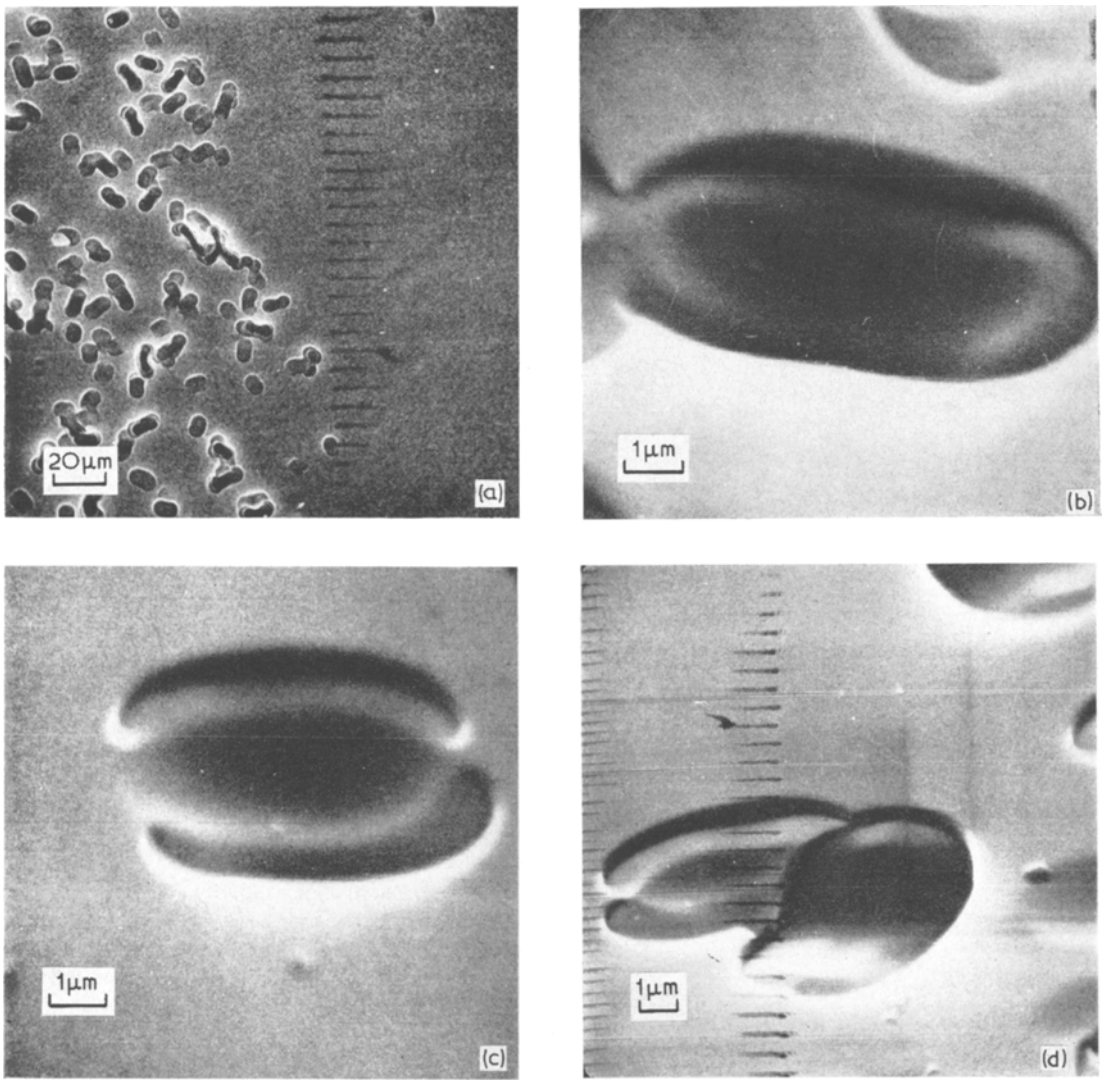

Figure 2 (a) The etch boundary between the polished surface and etched surface, of type fig. 1a, after an irradiation with $5 \times 10^{18}/cm^2$ 20 keV Ar^+ (b), (c) and (d). Various shallow formations in the etched region. Note the smooth central depression in all cases.

treat the problem in two parts, as indicated above: Firstly, to establish the possible equilibrium planes [6] which for the single-peaked "amorphous" sputtering curve are determined as having angles of incidence = 0°, 90° and θ_m, where θ_m represents the angle of incidence at which the maximum sputtering ratio occurs; secondly, to establish the final overall equilibrium state, by considering the motion of the intersections, which may result in certain formations disappearing [5]. Applying these ideas to the present pre-irradiation case of pits in glass which vary from having almost planar sides when lightly etched, to significantly concave surfaces when heavily etched, it follows that the former should expand with the sides moving out at a rate [5]

$$V = \frac{\phi}{n}(S_\theta - S_0)\cot\theta \qquad (1)$$

where ϕ = beam flux density, n = target atomic density, θ = angle of incidence on the steep

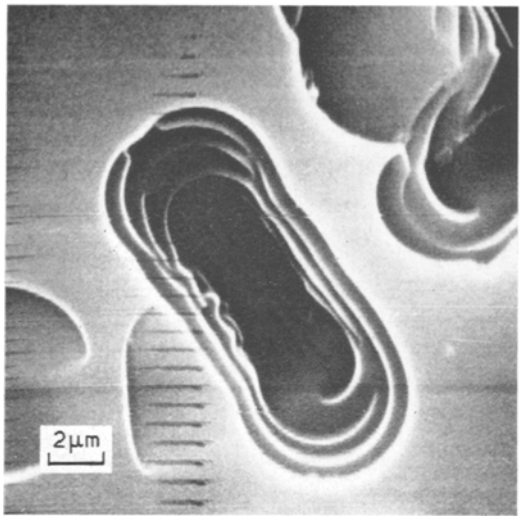

Figure 3 A deep Griffith flaw in the region shown in fig. 2, revealing the formation of a regular terraced structure.

sides, S_θ = sputtering coefficient at $\theta°$ incidence, and S_0 = sputtering coefficient of top surface (0°), forming flat-based pits, bordered by the steep smoothly curved sides. The variation of "intersection sputter-velocity", V, with the side angle, $\equiv \theta$ (fig. 5), can lead to various bowing effects when the sides of a pit vary in slope, and thus a good description is given of the kidney-shaped formations shown in fig. 2 except for the central depressions in the shallow pits and the terracing in the deeper pits, neither of which are predicted from the above theories. Considering the heavily etched surfaces: from the expression

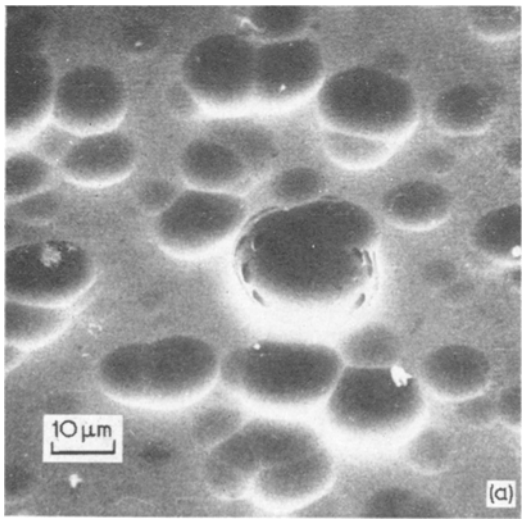

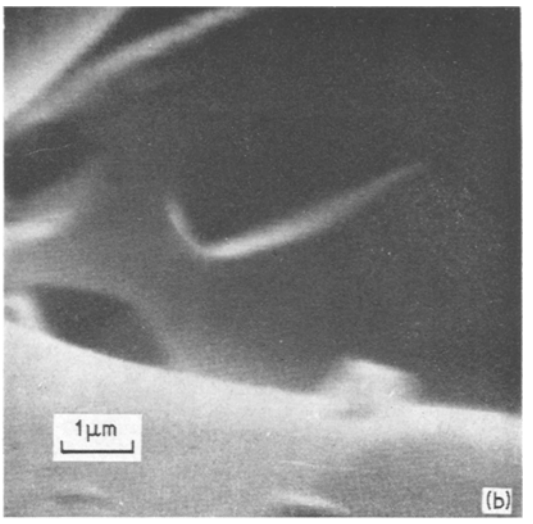

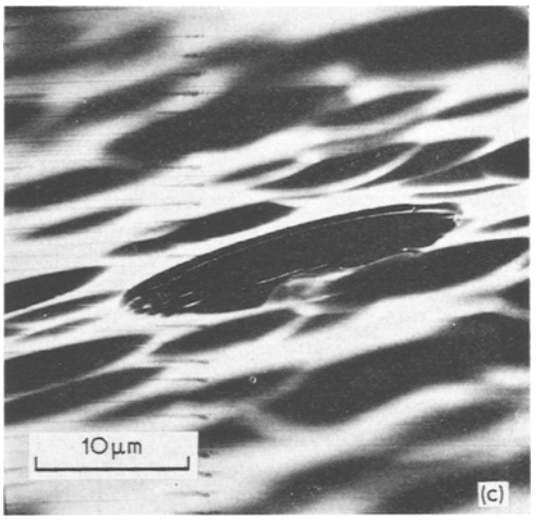

Figure 4 (a) The etched surface, of type fig. 1b, after irradiation with 5×10^{18}/cm^2 20 keV Ar^+, showing sharply defined steps cut into the deep central pit. (b) A close-up of a step in the central pit viewed at 75° to the surface normal. (c) A very deep pit, showing a continuous step at the rim, and a dense population of random steps on the steep slopes.

for the rate of rotation of the surface tangent due to sputtering [6]

$$\left(\frac{\partial\theta}{\partial t}\right)_x = -\frac{\phi}{n}\cos^2\theta\left(\frac{\partial S}{\partial\theta}\right)_\theta\left(\frac{\partial\theta}{\partial x}\right)_t \qquad (2)$$

where t = time and x = distance measured in the plane of incidence along the $\theta = 0°$ plane. It is seen that for a concave surface,

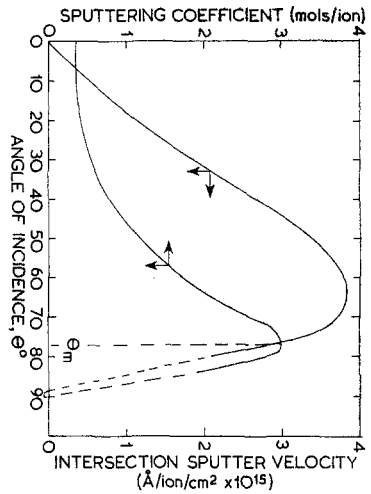

Figure 5 Sputtering data for 5.6 keV Ar^+ irradiation of silica glass (from Bach [1]), and the sputter velocity of an intersection between a plane at $\theta°$ and one at 0°, calculated from equation 1.

The Motion of Points A & B				
		initial	intermediate	final
A	$\dot{x}$	+ve, −ve	−ve	0
	$\dot{y}$	+ve, −ve	+ve	+ve
B	$\dot{x}$	+ve	+ve	+ve
	$\dot{y}$	+ve	+ve	+ve

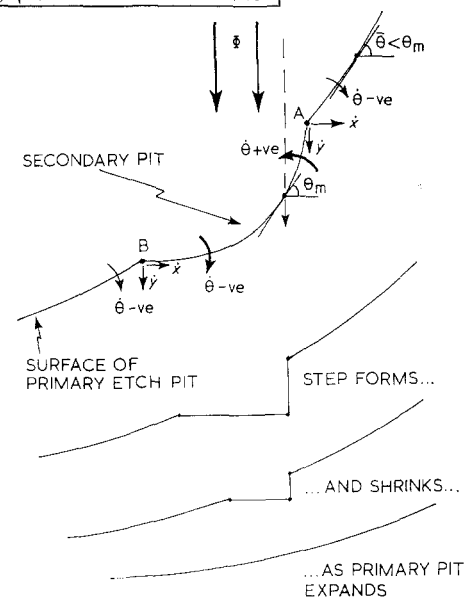

Figure 6 The formation of a step such as in fig. 4b due to secondary pits on slopes, θ, less than θ_m. The linear ($\dot{x}$, $\dot{y}$) and rotational ($\dot{\theta}$) motions are indicated by arrows and are predicted by equations 1 and 2. Thus, if the slope on the secondary pit exceeds θ_m a step forms.

($\partial\theta/\partial x$ is + ve), $\partial\theta/\partial t$ is − ve for $\theta < \theta_m$ since $\partial S/\partial\theta$ is + ve and thus the surface rotates to the equilibrium plane 0°, and for $\theta > \theta_m$, where $\partial S/\partial\theta$ is − ve the rotation is towards the 90° equilibrium plane. Therefore, pits where the initial slope passes through θ_m should develop 90° walls and 0° bases, while pits not reaching θ_m should expand until they reach 0°. A simple assumption that the sides of the (primary) pits were themselves initially slightly pitted and not perfectly smooth, would explain the appearance of the isolated steps, and their increasing numbers on steeper slopes, since the larger secondary pits could cause the local slope to exceed θ_m although the average slope be less (see fig. 6).

However, the continuous stepped rim appearing on the larger pits cannot be explained so simply. In fact the regularity in form of these rims and also of the terracing and central depressions observed in the lightly etched pits suggests a relationship with the initial regular geometries of the respective types of pit, which in turn suggests that some intrinsic properties of the sputtering process, other than basic variation of yield with angle, are responsible for these systematic developments.

3.2. Ion Reflection

It was suggested [5] that the peak in sputtering yield versus angle occurs when the angle of incidence reaches the critical reflection angle $\hat{\theta}$ given by

$$\Pi/2 - \hat{\theta} = \left\{\frac{5\Pi a_0^2\, n^{2/3}\, Z_1 Z_2 E_R}{(Z_1^{2/3} + Z_2^{2/3})^{\frac{1}{2}}\, E_i}\right\}^{\frac{1}{2}} \qquad (3)$$

the new symbols being a_0 = hydrogen Bohr radius, 0.53Å, Z_1 = ion atomic number, Z_2 = target species atomic number, E_R = Rydberg energy = 13.6 eV, and E_i = incident ion energy, above which angle the ion has a high probability of suffering a mirror reflection from the surface, with only a small energy transfer to the target. For the case of 5.6 keV Ar^+ on silica, assuming an average $Z_2 = 10$, the equation gives $\Pi/2 - \hat{\theta} = 77.9°$ which agrees very well with Bach's data ($\theta_m = 77°$) and for the present case $\Pi/2 - \hat{\theta} = 83.6°$. It has also been suggested that ion reflection could explain the pit which sometimes appears around the base of cone structures, observed frequently in some sputtering studies, where the cone half angle should be θ_m [5]. The reflected ion flux, retaining most of

the incident energy, adds to the primary flux around the cone base, causing a localised flux enhancement and the development of the pit. A very similar situation must exist with the lightly etched surface flaws in the present work, where the sides present a high angle for the incident ion flux (see fig. 7). Thus the base of the shallow flaws must initially receive a doubly enhanced flux as the reflected beams from opposite sides overlap. As the sides separate according to equation 1 the reflected beams will cease to overlap, leaving a smooth depression in the centre of the base, after which the expanding base formed by the separation of the sides is swept by a singly enhanced flux and finally eroded by the primary flux only. The central depression, being a shallow pit, and now eroded by the primary flux, will expand outwards as its radius of curvature increases, to the equilibrium 0° plane.

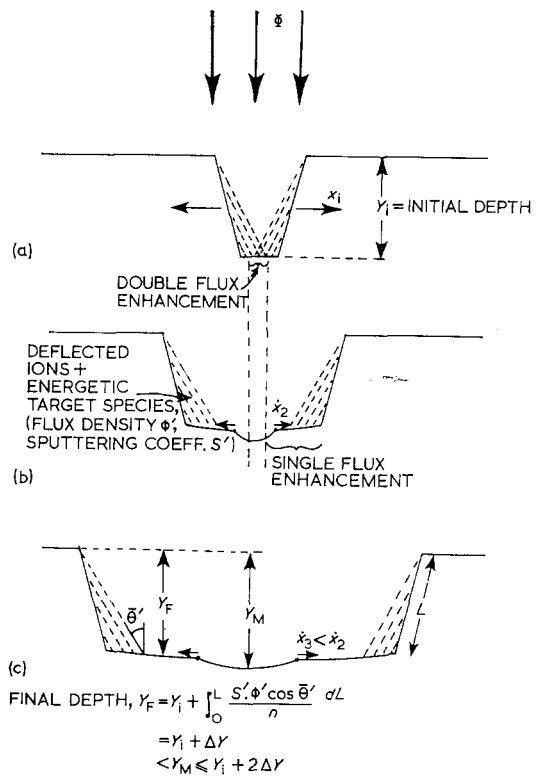

Figure 7 (a) A shallow surface flaw, having sides with slopes close to θ_m, experiences an additional energetic particle flux at the base due to quasi-specular reflection or re-emission of ions from both faces. (b) As the sides separate according to equation 1, the two secondary fluxes cease to overlap leaving a pit at the base centre. (c) This pit expands according to equations 1 and 2, while the flaw depth is increased over the rest of the base by the secondary flux from one side only.

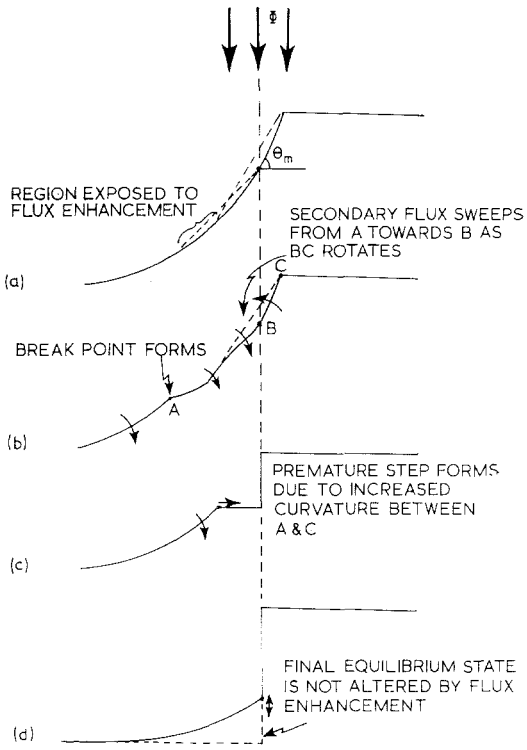

Figure 8 (a) A deep pit, as in fig. 4c, having a maximum slope initially exceeding θ_m experiences a flux enhancement over a narrow band of surface immediately below the steep slope which supplies the secondary flux. (b) This produces a depression, starting at A and progressing towards B as the side BC rotates to the 90° equilibrium state. (c) The increased curvature between A and B then results in a more rapid rotation to 0° according to equation 2, thus forming a step. (d) With BC now being at 90° the secondary flux ceases and the pit finally develops into the "pill-box" form predicted by equation 1.

Applying this concept to the case of a large pit (i.e. heavily etched) where the slopes do pass through θ_m, initially provides a reasonable explanation of the stepped rim see (fig. 8). In this case the reflected beam coming from a small band of surface for which $\theta \gtrsim \theta_m$ would strike the pit surface again lower down in a region where $\theta < \theta_m$ and begin an enhanced erosion over a small, well defined region. Any rotation of the ion-reflecting surface will be towards higher angles so that the reflected beam can only sweep *up* the slope and thus the enhanced erosion is confined to a narrow band of surface. Apart from increasing the rate of erosion

directly the effect is also to increase the term $\partial\theta/\partial x$ in equation 2 resulting in a more rapid approach to the equilibrium right angled-formation.

Since the reflected flux density is $\phi.\cos\theta.p(\theta)$, where $p(\theta)$ = probability of reflection, and $\cos\theta \to 0$ as $\theta \to 90°$ while $p(\theta) \to 1$ and the reflection ion energy $\to E_1$ as $\theta \to 90°$ the range of angles giving a significant energetic flux must be restricted to angles quite close to θ_m thus giving a well defined beam which allows the appearance of such sharply defined features as observed above. However, this concept is inadequate in explaining the terracing effect, where it appears that the flaw has developed sequentially in such a manner that the tops of the sides move out more rapidly than the lower regions and at the same time develop regular steps. Clearly another mechanism must operate.

3.3. The Sputtered Particle Flux

A notable fact about these deep flaws is that the two sides face each other in close proximity and must therefore be bombarded not only by the incident, and reflected, ion beam but also by a significant flux of sputtered particles emanating from the opposite surface. Various studies have been made of sputtered particles and it is known that the energy distribution is basically proportional to E^{-2}, and the angular distribution obeys, to a first approximation, a cosine law. However, Wehner [8] has found that, under normally incident bombardment, the mean sputtered particle energy is higher at 30° than at 0° ejection, while Andersen [9] finds the mean particle energy to increase with increasing angle of incidence. These facts are probably connected with the relationship between scattering angle and energy transfer in classical two body collisions which shows the energy transfer to increase monotonically with decreasing scattering angle (defined as the angle between velocity vectors of incident and struck particles before and after the collision respectively). This means that at high angles of incidence the high-energy sputtered particles, which must belong to early generations of recoil atoms, may still observe a close relationship between angle of ejection from the beam direction and energy. This relationship must become increasingly obscure as the ejection energy decreases, due to the rapidly increasing variety of collison sequences which contribute to that energy. This forward-peaked emission is indeed seen in the re-emergent incident-ion beam even when surface penetration occurs [10]

Thus it may be expected that the overall picture of the sputtered flux ranges from rather directional high energy components down to a truly random (cosine) distribution of low energy particles which constitute the vast majority of the total flux. The high energy particles will cause additional sputtering, but owing to the suggested asymmetric distribution this will tend to contribute to the flux enhancement effect described in the previous section. The size of this contribution will generally be small, e.g. for 41 keV Ar^+ sputtering of Au at 45° incidence $\sim$ 0.06 atoms/ion are produced with energies greater than 1 keV [11]. However, those particles with energies of the order of the surface binding energy ($\lesssim$ 10 eV) may simply redeposit on the opposite surface. Re-deposition would certainly help to explain why the flaws in the non-etched surface did not develop. The deep, lightly-

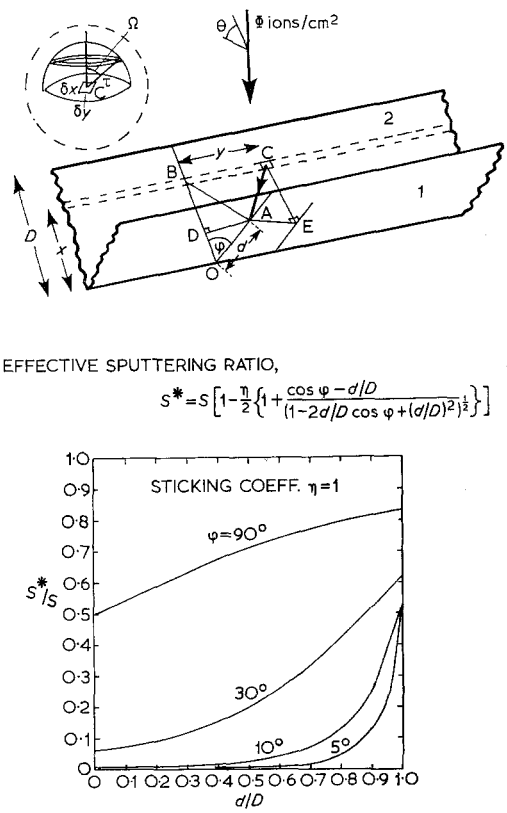

Figure 9 The effective sputtering ratio, S^*, at a point A on a plane (1) inclined symmetrically about the ion beam to a plane containing BCD, (2) when redeposition of the sputtered particles is taken into account, assuming a cosine spatial emission distribution.

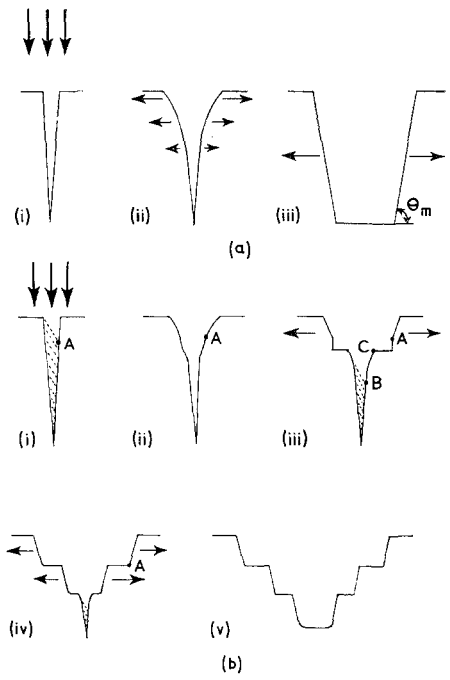

Figure 10 (a) (i) A deep surface flaw expanding due to sputtering, (ii) forms convex sides due to redeposition, (iii) which eventually form θ_m planes, when deposition becomes negligible, according to equation 2. (b) (i) With the additional secondary high energy flux the erosion rate is proportionally increased below point A, (ii) causing an "S" formation to appear with an inflection point near A. (iii) Equation 2 predicts the development of the convex surface into a θ_m plane and the concave surface into a step when secondary factors are neglected. Meanwhile the progressive separation of the sides cuts off the secondary flux between B and C and the cycle repeats itself. (iv) The "S" shape finally adopts a (0°, θ_m) configuration and the θ_m planes sweep outwards at a constant rate when redeposition is negligible. (v) Finally the sides are completely cut into a set of terraces sweeping out as a fixed formation.

etched flaws would experience a variation in net sputtering yield due to re-deposition (see fig. 9 and the appendix) which in the absence of secondary flux enhancement would cause a rapidly decreasing rate of separation with depth between points on opposite sides (fig. 10a). The secondary flux enhancement superimposed on this variation in sputtering rate causes a sharp increase in yield which produces a "wave" at the level where the incident secondary flux first appears (fig. 9b). This in turn affects the secondary flux distribution lower down on the opposite face, and so on until the faces are broken up into a series of waves, which develop more rapidly near the surface into sharply defined steps, and sequentially form the regular terraces as observed These mechanisms are illustrated in fig. 10.

4. Conclusion

In predicting the equilibrium topography evolving from an initially known surface, or in deducing the structure of a sample by sputter sectioning, allowance must be made, (a) when considering surfaces with slopes near, or greater than, the Lindhard critical angle, for the fluxes of reflected ions and high energy secondary particles, and (b) in certain cases for re-deposition of sputtered material.

Acknowledgements

The author wishes to acknowledge the helpful discussions had with Mr D. J. Elliott and Dr G. E. Chapman. Thanks are also due to Professors R. W. Cahn and M. W. Thompson, and Dr P. D. Townsend for their criticisms and suggestions during the preparation of this paper. Finally, the financial support from SRDE, Christchurch, Hants., is gratefully acknowledged.

Appendix (see fig. 9)

Deposition Rate of Low Energy Sputtered Particles from an Infinite Planar Strip onto an Adjacent Plane

Assume a cosine spatial emission distribution of sputtered particles from all points "C", i.e. $\phi = \phi_0 \cos \Omega$ (see top insert in fig. 9), then the total emitted flux from area $\delta x.\delta y$ at C is

$$\Phi.\cos\theta.S.\delta x.\delta y = \int_0^{\Pi/2} 2\Pi r.\sin\Omega.rd\Omega.\phi_0 \cos\Omega$$

$$= \Pi r^2 \phi_0$$

$$\therefore \phi_0 = \frac{\Phi.\cos\theta.S\ \delta x\ \delta y}{\Pi r^2}$$

where ϕ_0 = peak emitted flux density, Φ = incident ion flux density, θ = angle of incidence on plane BCO, Ω = angle of emission from plane BCO, and S = sputtering coefficient.

Then the flux density of sputtered particles from C arriving at A is

$$\phi_1 = \frac{\Phi \cos\theta S\ \delta x\ \delta y}{(AC)^2} \sin A\hat{C}D$$

and the resulting flux density on the plane at A is

$$\phi_1 \sin C\hat{A}E$$

$\therefore$ The total flux density striking the plane at A

from an infinite strip in the plane BCO parallel to the line of intersection is

$$\phi' = \int_{x_1}^{x_2}\int_{-\infty}^{\infty} \phi_1 \sin \hat{CAE}$$

$$= \int_{x_1}^{x}\int_{-\infty}^{\infty} \frac{\Phi.\cos\theta.S}{AC^2} \cdot \frac{d\sin\varphi}{AC} \cdot \frac{x\sin\varphi}{AC} \left(\frac{AC}{BC}\, d(AC)\right) dx$$

and using $AB/BC = \cos\xi\ (= \cos A\hat{C}B)$ gives

$$\phi' = \frac{\Phi.\cos\theta.S.r\sin^2\varphi}{\Pi}\int_{x_1}^{x_2}\int_0^{\Pi/2}\frac{\cos^2\xi\, d\xi}{AB^3}$$

$$= \frac{\Phi\cos\theta\, Sr\sin^2\varphi}{2}\int_{x_1}^{x_2}\frac{x}{(AB)^3}\, dx$$

$$= \frac{\Phi\cos\theta\, Sr\sin^2\varphi}{2}\int_{x_1}^{x_2} \frac{x\, dx}{((r\sin\varphi)^2 + (x - r\cos\varphi)^2)^{3/2}}$$

The substitution $y = x - r\cos\varphi$ converts this to the integrals:

$$\int \frac{\sinh\tau}{\cosh^2} \text{ and } \int \frac{d\tau}{\cosh^2\tau}$$

resulting in the final solution

$$\phi' = \frac{\Phi.\cos\theta.S}{2}\left\{\frac{\cos\varphi - r/x}{[1 - 2r/x\cos\varphi + (r/x)^2]^{\frac{1}{2}}}\right\}_{x_1}^{x_2}$$

Introducing a sticking coefficient η and considering the case of a V-shaped flaw of side D with $\theta = \varphi/2$ gives an effective sputtering rate S^* at A where $S^* = \Phi.\cos\theta.S - \phi'\eta$ is the net erosion rate
then

$$S^*/S = \left[1 - \eta/2 \left\{1 + \frac{\cos\varphi - d/D}{(1 - 2d/D\cos\varphi + (d/D)^2)^{\frac{1}{2}}}\right\}\right]$$

which is shown for $\eta = 1$ as a function of d/D for various φ, in fig. 9.

References

1. H. BACH, *J. Non-Cryst. Solids* **3** (1970) 1.
2. J. S. COLLIGON, Report on the Atomic Collisions in Solids Group Meeting, Sept. 1970, *Phys. Bull.* (Institute of Physics, London) **21** (1970) 518.
3. G. CARTER and J. S. COLLIGON, Ion Bombardment of Solids (Heinemann, London 1968).
4. R. G. WILSON, *Opt. and Laser Technol.* **2** (1970) 19.
5. A. D. G. STEWART and M. W. THOMPSON, *J. Mater. Sci.* **4** (1969) 61.
6. M. NOBES, J. S. COLLIGON, and G. CARTER, *ibid* **6** (1971) 115.
7. A. R. BAYLY and P. D. TOWNSEND, *Opt. and Laser Technol.* **2** (1970) 117.
8. G. K. WEHNER, *Phys. Rev.* **114** (1959) 1270.
9. H. H. ANDERSEN, Proc. Internat. Conf. Atomic Collision Phenomena in Solids p. 300 (North-Holland Amsterdam, London, 1970).
10. A. D. MARWICK, M. W. THOMPSON, B. W. FARMERY, and G. S. HARBINSON, to be published in Radiation Effects.
11. M. W. THOMPSON, *Phil. Mag.* **18** (1968) 377.

Received 10 June and accepted 22 September 1971.